A 27–46-GHz Low-Noise Amplifier With Dual-Resonant Input Matching and a Transformer-Based Broadband Output Network

Yaolong Hu, *Student Member, IEEE*, and Taiyun Chi, *Member, IEEE*

***Abstract*— This letter presents a 27–46-GHz low-noise amplifier (LNA) in a 45-nm CMOS silicon-on-insulator (SOI) process. Two circuit techniques are employed to enhance the LNA bandwidth. First, the intrinsic gate-to-drain parasitic capacitance of the input transistor and the frequency-dependent behavior of the first-stage load impedance are explored to realize dual resonances for S_{11}, thus extending the input matching bandwidth. Second, a network synthesis methodology is presented to convert a canonical second-order bandpass filter to a transformer-based output network, which realizes broadband power gain while occupying only one inductor footprint. In the measurements, the LNA 3-dB gain bandwidth is from 25.5 to 50 GHz with a peak gain of 21.2 dB at 37.8 GHz. The effective bandwidth of the LNA is limited by the 10-dB return loss bandwidth, which is from 27 to 46 GHz. The minimum noise figure (NF) is 2.4 dB at 27.8 GHz, and the NF remains <4.2 dB within the effective bandwidth. The measured IIP3 is −11.0 dBm at 38 GHz with 25.5-mW dc power consumption.**

***Index Terms*— 5G, broadband, CMOS, input matching, low-noise amplifier (LNA), millimeter-wave (mmWave), transformer.**

I. Introduction

THERE is a growing interest in exploring wideband transceivers (TRX) to simultaneously cover multiple millimeter-wave (mmWave) 5G bands around 28, 39, and 42 GHz [1]–[6]. Compared to narrowband implementations, broadband 5G TRX can enable unique application scenarios, including interband carrier aggregation, international roaming, and agile frequency hopping. In addition to high-speed wireless communication, emerging wireless sensing applications, such as 3-D mmWave imaging and radar, also favor broadband TRX frontends to improve the sensing spatial resolution.

One key challenge in designing broadband TRX is to extend the bandwidth of the low-noise amplifier (LNA) beyond conventional narrowband implementations. In this work, we aim to enhance the LNA bandwidth through two circuit innovations [see Fig. 1(a)]. First, we make use of the intrinsic gate-to-drain parasitic capacitance of the input transistor C_{gd1} and the frequency-dependent behavior of the first-stage load impedance Z_{L1} to realize dual resonances for the input reflection coefficient (S_{11}), thus broadening the input matching bandwidth [see Fig. 1(b)]. Second, we propose a network synthesis methodology that can miniaturize a canonical second-order bandpass filter into a single on-chip transformer footprint, serving as the broadband output network. It naturally absorbs the transformer nonideal magnetic coupling, finite winding inductances, and parasitic capacitances while achieving a uniform transimpedance gain across a wide frequency range.

Manuscript received February 6, 2021; accepted February 8, 2021. Date of publication February 15, 2021; date of current version June 7, 2021. This work was supported in part by the National Science Foundation under Grant CNS-1956297. *(Corresponding author: Yaolong Hu.)*

The authors are with the Department of Electrical and Computer Engineering, Rice University, Houston, TX 77005 USA (e-mail: yh72@rice.edu; taiyun.chi@rice.edu).

This article was presented at the IEEE MTT-S International Microwave Symposium (IMS 2021), Atlanta, GA, USA, June 6–11, 2021.

Color versions of one or more figures in this letter are available at https://doi.org/10.1109/LMWC.2021.3059592.

Digital Object Identifier 10.1109/LMWC.2021.3059592

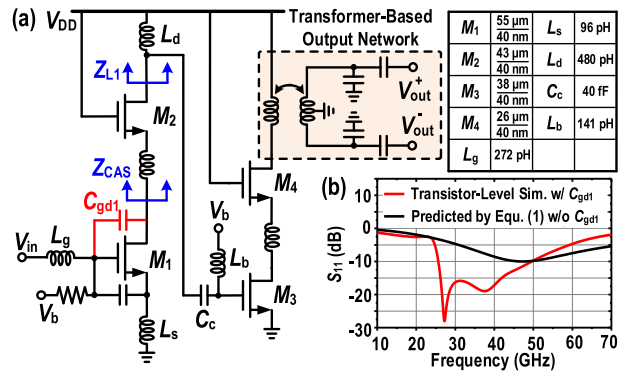

M_1	55 μm / 40 nm	L_s	96 pH
M_2	43 μm / 40 nm	L_d	480 pH
M_3	38 μm / 40 nm	C_c	40 fF
M_4	26 μm / 40 nm	L_b	141 pH
L_g	272 pH		

Fig. 1. (a) Schematic of the proposed broadband LNA. (b) Simulated dual-resonant input matching, including C_{gd1}, and predicted input matching based on (1) when neglecting C_{gd1}.

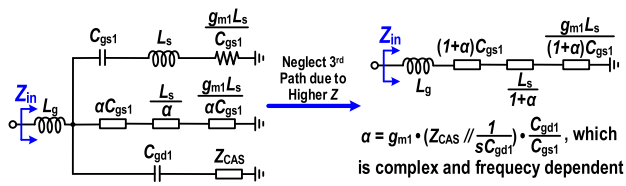

Fig. 2. Equivalent circuit of the input matching network, including C_{gd1}.

This letter is organized as follows. Section II elaborates on the design details of the dual-resonant input matching and transformer-based broadband output network. Section III presents the measurement results. Section IV concludes this letter with a performance comparison table.

II. Broadband LNA Implementation

A. Dual-Resonant Input Matching

The most frequently used mmWave LNA topology is the common source with inductive degeneration [7]–[15]. Neglecting the gate-to-drain parasitic capacitance C_{gd} of the input transistor, the input impedance is derived as

$$Z_{in}(s) = \frac{1}{sC_{gs}} + (L_g + L_s)s + \frac{g_m L_s}{C_{gs}} \tag{1}$$

where L_g is the series gate inductance, L_s is the degeneration inductance, and C_{gs} is the gate-to-source capacitance [16].

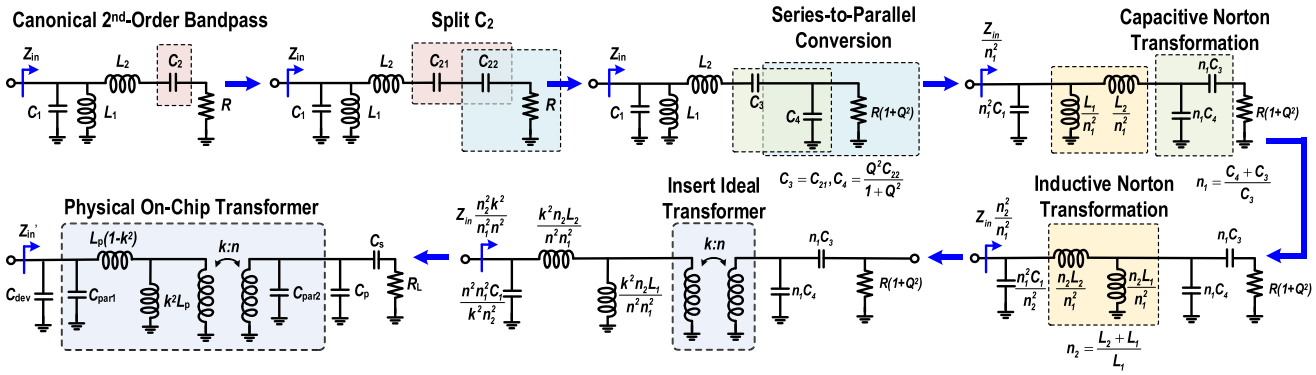

Fig. 3. Synthesis procedure to miniaturize a canonical second-order bandpass filter into a single-transformer footprint for the broadband output network.

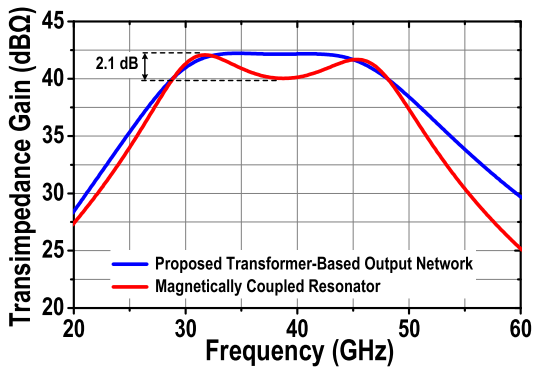

Fig. 4. Transimpedance gain comparison between the proposed transformer-based second-order bandpass output network and a carefully designed magnetically coupled resonator with similar 3-dB bandwidth.

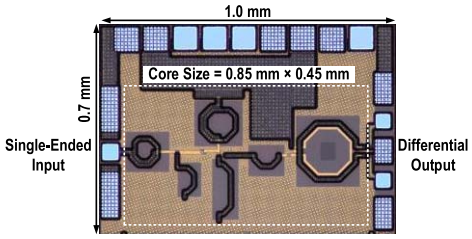

Fig. 5. LNA micrograph.

As shown in (1), the input impedance consists of a series LC resonance and a frequency-independent real part. As such, it can only achieve a single S_{11} resonance, resulting in limited input matching bandwidth [see Fig. 1(b)]. One may improve the input matching bandwidth by employing a high-order matching network. However, it usually involves multiple inductors at the LNA input, resulting in a compromised noise figure (NF).

Although neglecting C_{gd} has little effect on the input matching condition for low-gigahertz LNAs, the input impedance predicted by (1) certainly deviates from transistor-level simulations at mmWave, as shown in Fig. 1(b). To address this issue, we rederive the equivalent circuit of the input matching network, including C_{gd1} (see Fig. 2). The equivalent circuit consists of three parallel paths in series with L_g. The first path is the same as in the conventional common source with inductive degeneration topology. The second path is a scaled version of the first path with a coefficient of α. The expression of α is shown in Fig. 2, which is a function of the transistor intrinsic parameters (g_{m1}, C_{gs1}, and C_{gd1}) and the impedance looking into the upper cascode node Z_{CAS}. The third path models the feedforward current through C_{gd1}, which remains a higher impedance than the other two within the frequency of interest. We neglect the third path in our analysis and consolidate the first two paths, as shown in Fig. 2.

The key to achieve broadband input matching is to explore the frequency-dependent behavior of Z_{L1}, Z_{CAS}, and α. A simplified yet intuitive design procedure to synthesize dual-resonant S_{11} at two desired frequencies f_1 and f_2 is summarized as follows. First, the size and biasing of the input transistor are chosen based on the dc power budget and NF_{min} versus biasing simulation. Therefore, the intrinsic parameters of the input transistor, i.e., g_{m1}, C_{gs1}, and C_{gd1} are determined. Next, we assume that the first-stage load impedance Z_{L1} has a single resonance around f_1. The purpose of this assumption is to differentiate the value of Z_{CAS} at the two S_{11} resonances, i.e., set Z_{CAS} as a high impedance at f_1 but a low impedance at f_2, allowing us to optimize the two S_{11} resonances sequentially. Beginning with the high-frequency resonance at f_2, as Z_{CAS} is a low impedance and much smaller than $1/2\pi f_2 C_{gd1}$, α becomes purely real. The values of L_g, L_s, and g_{m2} can then be determined from the equivalent circuit in Fig. 2 by setting series LC resonance at f_2 and the real part of Z_{in} close to 50 Ω. The only undetermined circuit parameters for the first stage are the passive elements in the load network, i.e., L_d, C_c, and L_b in Fig. 1. Their values can be derived based on the conditions to achieve Z_{L1} resonance around f_1 and close to 50 Ω for the real part of Z_{in}.

Following the procedure described above, the simulated $f_1 = 27.1$ GHz and the simulated $f_2 = 39.5$ GHz, which is very close to our targeted values of 27 and 41 GHz. Although our proof-of-concept implementation targets at the 28 GHz/39 GHz/42 GHz 5G bands, the theoretical framework to achieve dual-resonant S_{11} presented in this section can be readily extended to mmWave LNA designs at other frequency bands.

B. Transformer-Based Broadband Output Network

In addition to dual-resonant input matching, the output load network also plays an essential role in achieving a broadband LNA gain. As the cascode second stage can be modeled as a current source with a high output impedance, the design goal of the output network is to deliver a uniform transimpedance gain within the frequency of interest while absorbing the parasitic capacitance of the second stage.

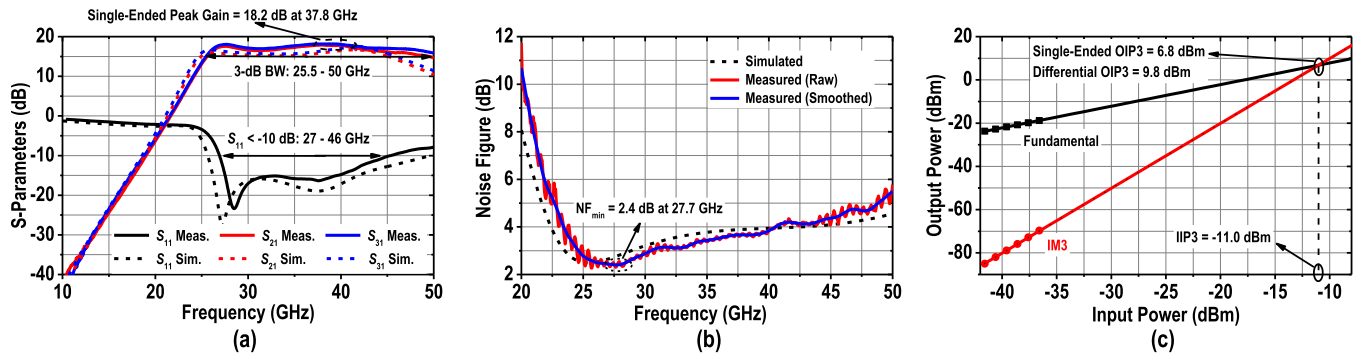

Fig. 6. (a) Measured and simulated S-parameters. (b) Measured and simulated NF. (c) Measured IIP3 and OIP3 at 38 GHz.

Starting with a canonical second-order bandpass filter, the output network synthesis procedure is summarized in Fig. 3. First, we split the capacitor C_2 into two series capacitors C_{21} and C_{22} and perform a series-to-parallel conversion for C_{22} and the load resistor R. Note that a low quality factor ($Q = 1/\omega C_{22} R$) is desired to broaden the bandwidth of the series-to-parallel conversation. Next, we apply two Norton transformations to the series–shunt capacitors and shunt–series inductors. The two transformation ratios n_1 and n_2 are highlighted in Fig. 3. Finally, we insert an ideal transformer with a turn ratio of $k{:}n$ into the network and merge it with the series and shunt inductors and the shunt capacitors as a physical on-chip transformer.

The above network synthesis methodology naturally utilizes the transformer nonideal magnetic coupling, finite winding inductances, and parasitic capacitances to achieve second-order bandpass filtering while occupying only a single inductor footprint [17], [18]. It also serves as an output balun, making the LNA easier to be employed in an mmWave RX chain, where the following building blocks, such as phase shifter, variable-gain amplifier, and mixer, are mostly designed in a differential manner. As the proposed network is derived from a canonical second-order bandpass filter, its bandwidth and gain flatness outperform commonly used magnetically coupled resonators [19], as illustrated in Fig. 4.

III. Measurement Results

The broadband LNA is implemented in a 45-nm CMOS silicon-on-insulator (SOI) process (see Fig. 5). The supply voltage is 1.3 V with a dc current of 19.6 mA, resulting in 25.5-mW dc power consumption.

Fig. 6 summarizes the small-signal, NF, and linearity measurement results. The effective LNA bandwidth is defined as the intersection of the 3-dB gain bandwidth and 10-dB return loss bandwidth [20], which is from 27 to 46 GHz. The single-ended peak gain is 18.2 dB at 37.8 GHz, resulting in a differential peak gain of 21.8 dB. The gain ripple within the effective bandwidth is 1.2 dB. The measured common-mode rejection ratio (CMRR) is >24 dB, which indicates that the LNA differential outputs are well balanced. The measured common-mode and differential-mode stability factors (K) are greater than 1. For the NF measurements, the minimum NF is 2.4 dB at 27.7 GHz, and the NF remains <4.2 dB within the effective bandwidth [see Fig. 6(b)]. For the IIP3 measurement, two tones at 38 and 38.1 GHz are applied to the LNA input with a power level from −41.6 to −36.6 dBm. The measured IIP3 is −11.0 dBm, and the differential OIP3 is 9.8 dBm [see Fig. 6(c)].

TABLE I

Performance Summary and Comparison

	JSSC 2020 [20]		RFIC 2019 [21]		GSMM 2018 [22]	IMS 2018 [23]	**This Work**
BW_{eff}* (GHz)	22-32	22-32	24-29†	37-42†	27-47.5†	26-28†	**27-46**
3-dB BW (GHz)	19-36	20-36	24-29†	37-42†	24-47.5	14-31	**25.5-50**
Peak Gain (dB)	21.5	17.9	19.1†	23	20	14	**21.2**
NF (dB)	1.7-2.2	2.1-2.9	3.1-3.7		4.2-5.5	1.3-1.6	**2.4-4.2**
IIP3 (dBm)	-13.4	-14.4	-13.2	-19	-9.4††	+4†	**-11**
P_{dc} (mW)	17.3	5.6	20.5		58	15	**25.5**
Core Size (mm^2)	0.05		0.22		0.2	0.3	**0.38**
FoM**	24.7	30.8	3.8	1.1	7.0	178.3	**26.1**
Tech.	22-nm FDSOI		22-nm FDSOI		45-nm RFSOI	45-nm RFSOI	**45-nm RFSOI**

* Intersection of 3-dB gain BW and 10-dB return loss BW.
† Graphically estimated. †† Estimated using IP_{1dB} + 9.6dB.
** $\text{FoM} = \frac{10^3 \times Gain[\frac{V}{V}] \times BW_{eff}[GHz] \times IIP3[mW]}{P_{dc}[mW] \times (NF[linear]-1) \times f_c[GHz]}$. f_c is the geometric mean.
Peak gain and NF_{min} are taken in FoM calculation.

IV. Conclusion

This letter presents a 27–46 GHz broadband LNA design. Leveraging the intrinsic gate-to-drain parasitic capacitance of the input transistor and the frequency-dependent behavior of the first-stage load impedance, we realize dual resonances for S_{11}, hence extending the input matching bandwidth. We also develop a network synthesis flow that converts a canonical second-order bandpass filter to a transformer-based output network to extend the 3-dB gain bandwidth and guarantee the gain flatness. Table I summarizes our LNA performance and compares it with state-of-the-art LNAs at a similar operating frequency. Our design achieves the highest 3-dB gain bandwidth (25.5–50 GHz) and a very competitive Figure-of-Merit.

Acknowledgment

The authors would like to thank GlobalFoundries for chip fabrication and members of the Rice Integrated Systems and Electromagnetics (RISE) Lab for helpful technical discussions.

REFERENCES

[1] M.-Y. Huang, T. Chi, S. Li, T.-Y. Huang, and H. Wang, "A 24.5–43.5-GHz ultra-compact CMOS receiver front end with calibration-free instantaneous full-band image rejection for multiband 5G massive MIMO," *IEEE J. Solid-State Circuits*, vol. 55, no. 5, pp. 1177–1186, May 2020.

[2] M.-Y. Huang, T. Chi, F. Wang, S. Li, T.-Y. Huang, and H. Wang, "A 24.5–43.5GHz compact RX with calibration-free 32–56dB full-frequency instantaneously wideband image rejection supporting multi-Gb/s 64-QAM/256-QAM for multi-band 5G massive MIMO," in *Proc. IEEE Radio Freq. Integr. Circuits Symp. (RFIC)*, Jun. 2019, pp. 275–278.

[3] L. Gao and G. M. Rebeiz, "A 22–44-GHz phased-array receive beamformer in 45-nm CMOS SOI for 5G applications with 3–3.6-dB NF," *IEEE Trans. Microw. Theory Techn.*, vol. 68, no. 11, pp. 4765–4774, Nov. 2020.

[4] M. Lokhandwala, L. Gao, and G. M. Rebeiz, "A high-power 24–40-GHz transmit–receive front end for phased arrays in 45-nm CMOS SOI," *IEEE Trans. Microw. Theory Techn.*, vol. 68, no. 11, pp. 4775–4786, Nov. 2020.

[5] A. A. Alhamed, O. Kazan, and G. M. Rebeiz, "A multi-standard 15-57 GHz 4-channel receive beamformer with 4.8 dB midband NF for 5G applications," in *IEEE MTT-S Int. Microw. Symp. Dig.*, Aug. 2020, pp. 1011–1014.

[6] S. Mondal, R. Singh, and J. Paramesh, "21.3 A reconfigurable bidirectional 28/37/39GHz front-end supporting MIMO-TDD, carrier aggregation TDD and FDD/full-duplex with self-interference cancellation in digital and fully connected hybrid beamformers," in *IEEE Int. Solid-State Circuits Conf. (ISSCC) Dig. Tech. Papers*, Feb. 2019, pp. 348–349.

[7] M.-Y. Huang, T. Chi, F. Wang, T.-W. Li, and H. Wang, "A full-FoV autonomous hybrid beamformer array with unknown blockers rejection and signals tracking for low-latency 5G mm-wave links," *IEEE Trans. Microw. Theory Techn.*, vol. 67, no. 7, pp. 2964–2974, Jul. 2019.

[8] M.-Y. Huang, T. Chi, F. Wang, T.-W. Li, and H. Wang, "A 23-to-30GHz hybrid beamforming MIMO receiver array with closed-loop multistage front-end beamformers for full-FoV dynamic and autonomous unknown signal tracking and blocker rejection," in *IEEE Int. Solid-State Circuits Conf. (ISSCC) Dig. Tech. Papers*, Feb. 2018, pp. 68–69.

[9] P. Qin and Q. Xue, "Compact wideband LNA with gain and input matching bandwidth extensions by transformer," *IEEE Microw. Wireless Compon. Lett.*, vol. 27, no. 7, pp. 657–659, Jul. 2017.

[10] M. Elkholy, S. Shakib, J. Dunworth, V. Aparin, and K. Entesari, "A wideband variable gain LNA with high OIP3 for 5G using 40-nm bulk CMOS," *IEEE Microw. Wireless Compon. Lett.*, vol. 28, no. 1, pp. 64–66, Jan. 2018.

[11] C. Li *et al.*, "5G mm-wave front-end-module design with advanced SOI process," in *Proc. IEEE 12th Int. Conf. ASIC (ASICON)*, Oct. 2017, pp. 1017–1020.

[12] T. Chi, J. S. Park, S. Li, and H. Wang, "A millimeter-wave polarization-division-duplex transceiver front-end with an on-chip multifeed self-interference-canceling antenna and an all-passive reconfigurable canceller," *IEEE J. Solid-State Circuits*, vol. 53, no. 12, pp. 3628–3639, Dec. 2018.

[13] T. Chi, J. S. Park, S. Li, and H. Wang, "A 64GHz full-duplex transceiver front-end with an on-chip multifeed self-interference-canceling antenna and an all-passive canceler supporting 4Gb/s modulation in one antenna footprint," in *IEEE Int. Solid-State Circuits Conf. (ISSCC) Dig. Tech. Papers*, Feb. 2018, pp. 76–77.

[14] S. Li, T. Chi, and H. Wang, "Multi-feed antenna and electronics co-design: An E-band antenna-LNA front end with on-antenna noise-canceling and gm-boosting," *IEEE J. Solid-State Circuits*, vol. 55, no. 12, pp. 3362–3375, Dec. 2020.

[15] S. Li, T. Chi, D. Jung, T.-Y. Huang, M.-Y. Huang, and H. Wang, "4.2 an E-vand high-linearity antenna-LNA front-end with 4.8dB NF and 2.2dBm IIP3 exploiting multi-feed on-antenna noise-canceling and gm-boosting," in *IEEE Int. Solid-State Circuits Conf. (ISSCC) Dig. Tech. Papers*, Feb. 2020, pp. 78–79.

[16] B. Razavi, *RF Microelectronics*, 2nd ed. New York, NY, USA: Prentice-Hall, 2012.

[17] J. R. Long, "Monolithic transformers for silicon RF IC design," *IEEE J. Solid-State Circuits*, vol. 35, no. 9, pp. 1368–1382, Sep. 2000.

[18] H. Wang, C. Sideris, and A. Hajimiri, "A CMOS broadband power amplifier with a transformer-based high-order output matching network," *IEEE J. Solid-State Circuits*, vol. 45, no. 12, pp. 2709–2722, Dec. 2010.

[19] M. Vigilante and P. Reynaert, "On the design of wideband transformer-based fourth order matching networks for *E*-band receivers in 28-nm CMOS," *IEEE J. Solid-State Circuits*, vol. 52, no. 8, pp. 2071–2082, Aug. 2017.

[20] B. Cui and J. R. Long, "A 1.7-dB minimum NF, 22–32-GHz low-noise feedback amplifier with multistage noise matching in 22-nm FD-SOI CMOS," *IEEE J. Solid-State Circuits*, vol. 55, no. 5, pp. 1239–1248, May 2020.

[21] L. Gao and G. M. Rebeiz, "A 24–43 GHz LNA with 3.1–3.7 dB noise figure and embedded 3-Pole elliptic high-pass response for 5G applications in 22 nm FDSOI," in *Proc. IEEE Radio Freq. Integr. Circuits Symp. (RFIC)*, Jun. 2019, pp. 239–242.

[22] V. Chauhan and B. Floyd, "A 24–44 GHz UWB LNA for 5G cellular frequency bands," in *Proc. 11th Global Symp. Millim. Waves (GSMM)*, May 2018, pp. 1–3.

[23] C. Li, O. El-Aassar, A. Kumar, M. Boenke, and G. M. Rebeiz, "LNA design with CMOS SOI process-l.4dB NF K/Ka band LNA," in *IEEE MTT-S Int. Microw. Symp. Dig.*, Jun. 2018, pp. 1484–1486.